Energy & Environmental Science

www.rsc.org/ees

Volume 6 | Number 5 | May 2013 | Pages 1341–1642

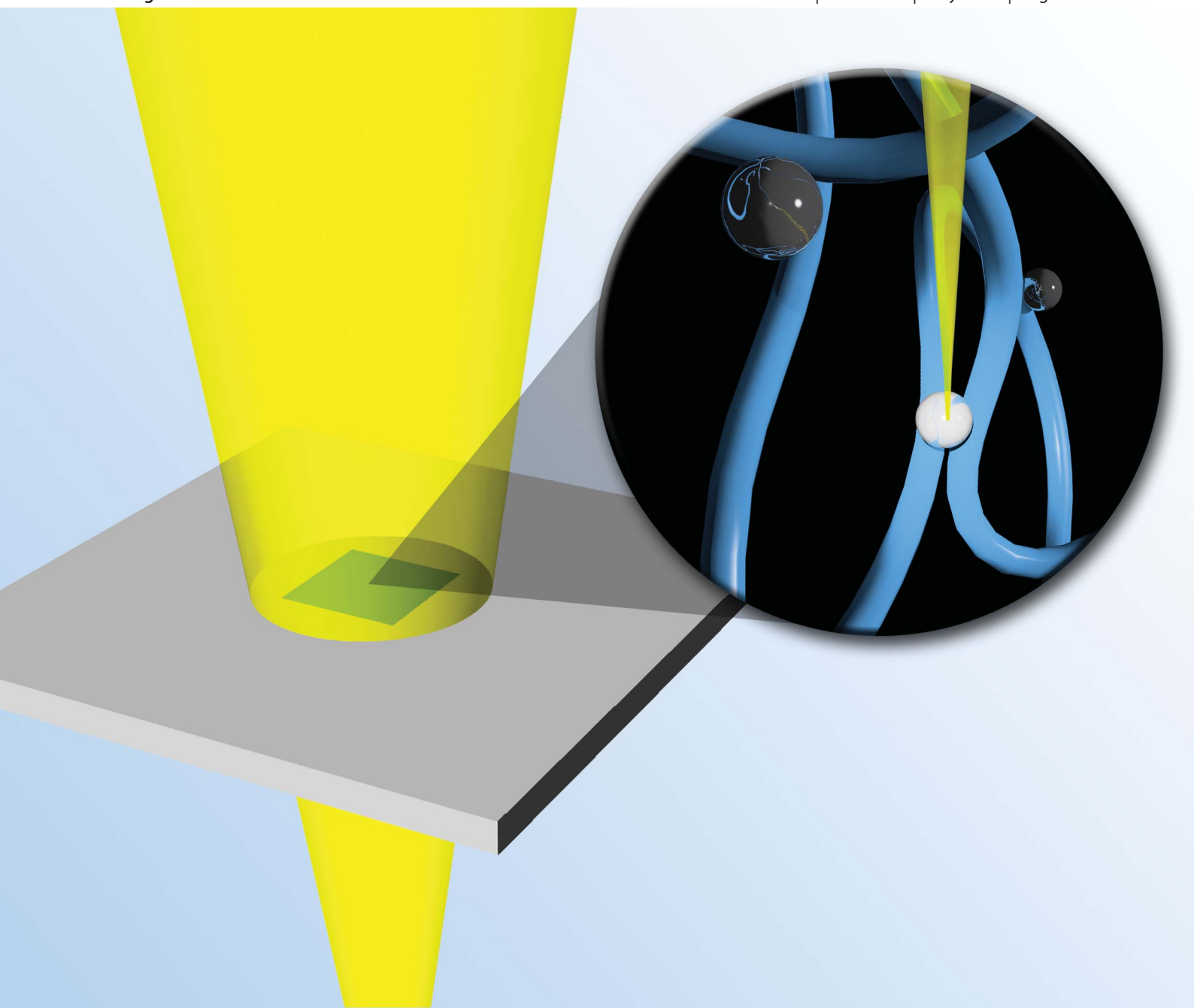

ISSN 1754-5692

RSC Publishing

PAPER

Darling *et al.*

Detection and role of trace impurities in high-performance organic solar cells

Energy & Environmental Science

RSC Publishing

PAPER

Detection and role of trace impurities in high-performance organic solar cells†

Cite this: *Energy Environ. Sci.*, 2013, **6**, 1513

Maxim P. Nikiforov,‡[a] Barry Lai,[b] Wei Chen,[cd] Si Chen,[b] Richard D. Schaller,[ae] Joseph Strzalka,[b] Jörg Maser[b] and Seth B. Darling*[ad]

Received 18th February 2013
Accepted 18th March 2013

DOI: 10.1039/c3ee40556g

www.rsc.org/ees

Trace impurities in organic solar cells, such as those from residual catalyst material in conjugated polymers, are often ignored but are known to deleteriously affect device performance. Batch-to-batch variations in the nature and quantity of such impurities leads to widespread issues with irreproducible optoelectronic function, yet to date no technique has emerged that is reliably capable of identifying the character of impurities or their concentration in organic photovoltaic active layer blends. Here we focus on state-of-the-art, high-performance bulk heterojunction blends and show that synchrotron-based X-ray fluorescence can detect and quantify trace concentrations of metal impurities in these systems. Adopting a strategy of artificially introducing known quantities of additional catalyst into polymer/fullerene blends, we identify both the threshold concentration at which performance degrades and the mechanism for the degradation. With the knowledge of a target impurity concentration and a technique in hand to accurately measure their presence, researchers can implement materials preparation processes to achieve consistent, high performance in organic solar cells.

Broader context

Organic solar cells are in the midst of a period of dramatic performance improvements and appear increasingly likely to assume a significant role in renewable energy production in the future. Batch-to-batch variations in performance are a well-known challenge in the field, yet in most cases the underlying reasons for these variations are not known. The polymers used in the majority of high-performance devices are synthesized using coupling reactions catalyzed by transition metal complexes, and residual amounts of these catalysts leftover in the final products can substantially affect device efficiency. In this article, we present a technique that is capable—for the first time—of quantitatively detecting trace amounts of metal impurities in organic photovoltaic materials. With such a tool in hand, researchers have the ability to work with reproducible materials and also perhaps to push performance to new levels.

Introduction

The field of organic solar cells is in the midst of a period of remarkable progress. Tremendous increases in power conversion efficiency[4–9] coupled with the low cost, scalability,[10] and environmentally benign[11] nature of organic photovoltaics (OPVs) have positioned this technology on the cusp of genuine impact in the energy marketplace. The vast majority of conjugated polymers in high-performance OPVs are synthesized *via* Stille[12,13] or Suzuki[14] coupling reactions catalyzed by palladium complexes (Fig. 1). Though generally overlooked, residual catalyst or palladium nanoparticles resulting from catalyst degradation[15] are extraordinarily difficult to remove from the end product as they bind to conjugated polymers as well as to some small molecules used in organic optoelectronics. Further complicating the situation is the fact that the extent of palladium contamination will vary not only between synthetic schemes due to differences in affinity for palladium but also batch-to-batch, making large-scale commercialization a daunting challenge. Indeed, it is likely that this variability represents a significant contribution to the oft observed irreproducibility of organic solar cell efficiencies when using different batches of polymer. An analogous situation exists with other metal impurities resulting from alternate synthetic processes (Sonogashira,[16] Yamomoto,[17] Kumada,[17] *etc.*). These metal impurities are also often associated with deterioration in solubility.[18] Making matters worse, palladium contamination is at a level that is typically undetectable by conventional analytical techniques, such as nuclear magnetic resonance (NMR), optical absorption, Fourier transform infrared spectroscopy (FTIR), or gel permeation chromatography (GPC), used by organic chemists for the determination of material purity; yet, even at these

[a]*Argonne National Laboratory, Center for Nanoscale Materials, 9700 S. Cass Ave., Argonne, Illinois 60439, USA. E-mail: darling@anl.gov; Fax: +1 630-252-4646; Tel: +1 630-252-4580*

[b]*Argonne National Laboratory, X-ray Science Division, Argonne, Illinois, USA*

[c]*Argonne National Laboratory, Materials Science Division, Argonne, Illinois, USA*

[d]*The University of Chicago, Institute for Molecular Engineering, Chicago, Illinois, USA*

[e]*Northwestern University, Department of Chemistry, Evanston, Illinois, USA*

† Electronic supplementary information (ESI) available: X-ray reflectivity data used for measurement of film thickness. See DOI: 10.1039/c3ee40556g

‡ Current address: HGST, San Jose, California, USA.

This journal is © The Royal Society of Chemistry 2013

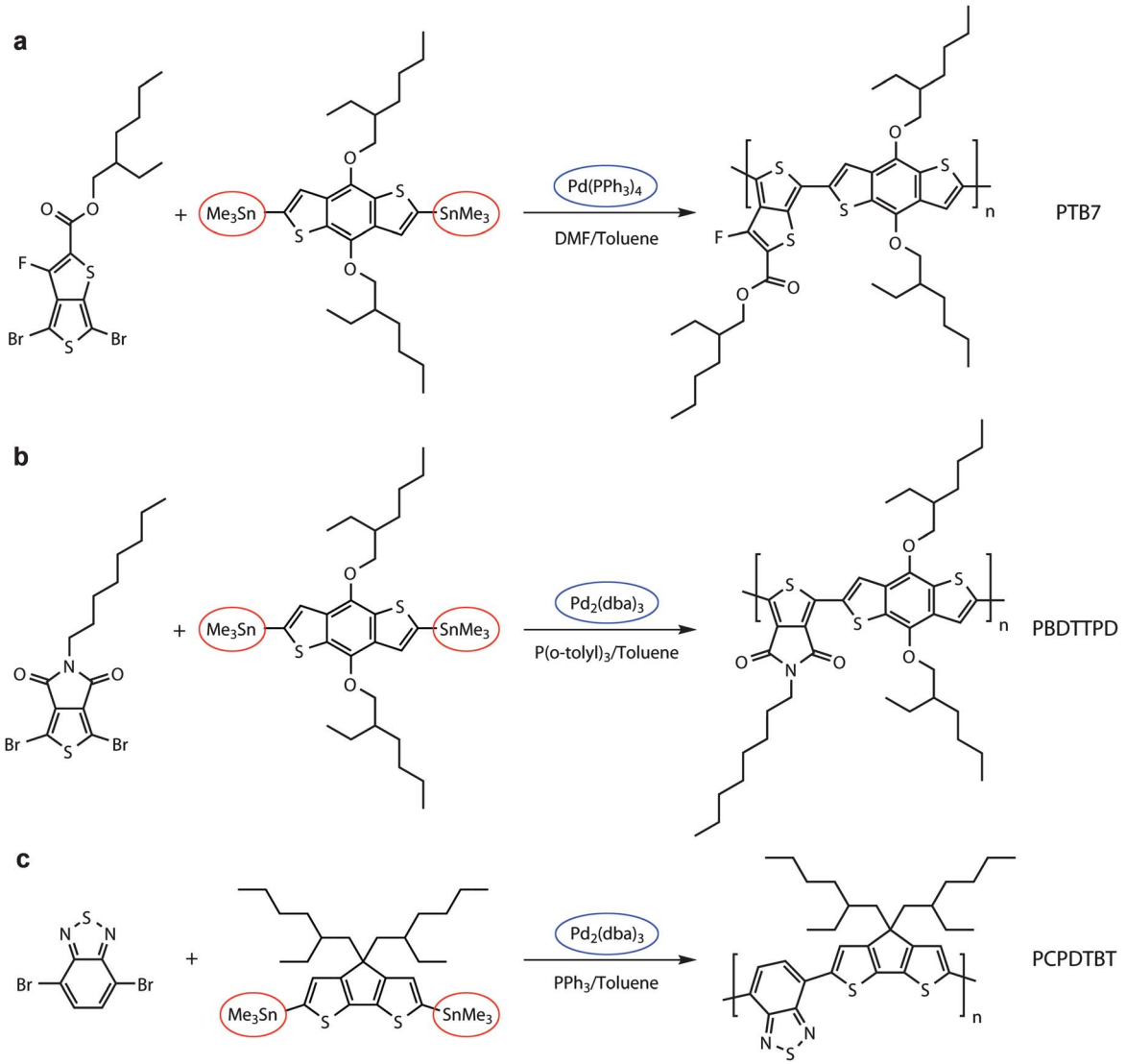

Fig. 1 Synthetic schemes for three high-performance conjugated polymers used in organic solar cells: (a) PTB7,[23] (b) PBDTTPD,[24] and (c) PCPDTBT.[25] The use of tin and palladium is ubiquitous in this class of materials due to the Stille coupling reaction.

low concentrations, palladium and other metal impurities can have dramatic effects on device performance.[1,3,19–22] Researchers have generally turned to electronic measurements of devices in order to try to indirectly back out the impurity concentration,[2,19] which for techniques such as time-resolved microwave conductivity has proven ineffective.[22] Therefore, a measurement technique capable of directly and quantitatively detecting the presence of trace palladium and other metal impurities in organic optoelectronic systems is sorely needed. Here we demonstrate the utility of synchrotron-based X-ray fluorescence for quantitative determination of the amount of palladium and other metal impurities in high-performance OPV polymers and bulk heterojunction polymer/fullerene blends.

Results and discussion

It has been reported that palladium concentrations as low as ~0.05 wt% can adversely affect OPV performance in lower efficiency devices;[19] other metal impurities can have dramatic effects on the performance as well.[1,3,19–22] To determine both the threshold for and nature of palladium influence on high-performance organic solar cells, we prepared polymer/fullerene bulk heterojunction solar cells from both original source PTB7 and polymer with varying amounts of added pristine tetrakis-(triphenylphosphine)palladium(0) ($Pd(PPh_3)_4$) catalyst. Current–voltage (J–V) curves for these devices are displayed in Fig. 2, with the relevant device parameters (short circuit current, J_{sc}; open circuit voltage, V_{oc}; fill factor, FF; power conversion efficiency, PCE) plotted individually in Fig. 3a on a logarithmic scale of added palladium catalyst concentration. Fig. 3b presents these data on a normalized scale to show the relative influence on each parameter. From these data, one can see that V_{oc} is the first parameter to display a detrimental effect from palladium impurities, decreasing when the added palladium concentration (in solution) is still below 1%. FF is the next parameter to show an effect, with notable kinks forming in the J–V curve at higher

 This journal is © The Royal Society of Chemistry 2013

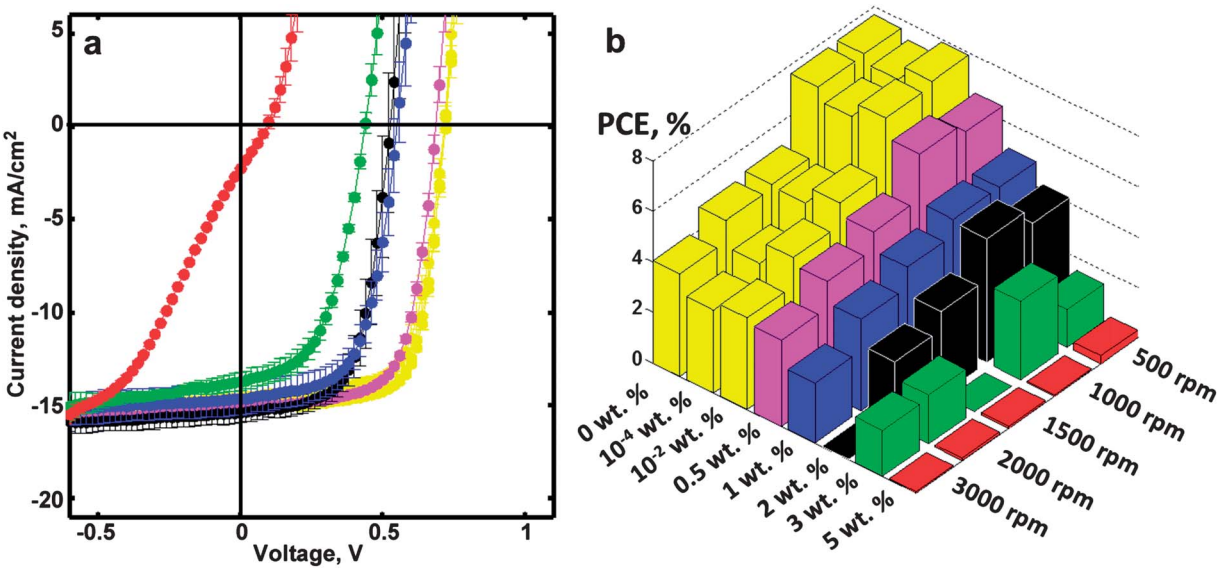

Fig. 2 (a) Current–voltage data from PTB7/$PC_{71}BM$ solar cells having various amounts $Pd(PPh_3)_4$ catalyst added to the active layer blend (spin cast at 1000 rpm). (b) Summary of PCE as a function of both spin speed and added palladium catalyst concentration in solution. Color scheme: red – 5 wt%; green – 3 wt%; black – 2 wt%; blue – 1 wt%; magenta – 0.5 wt%; yellow – <0.1 wt%. Error bars represent the spread of values from an average of 3–4 devices.

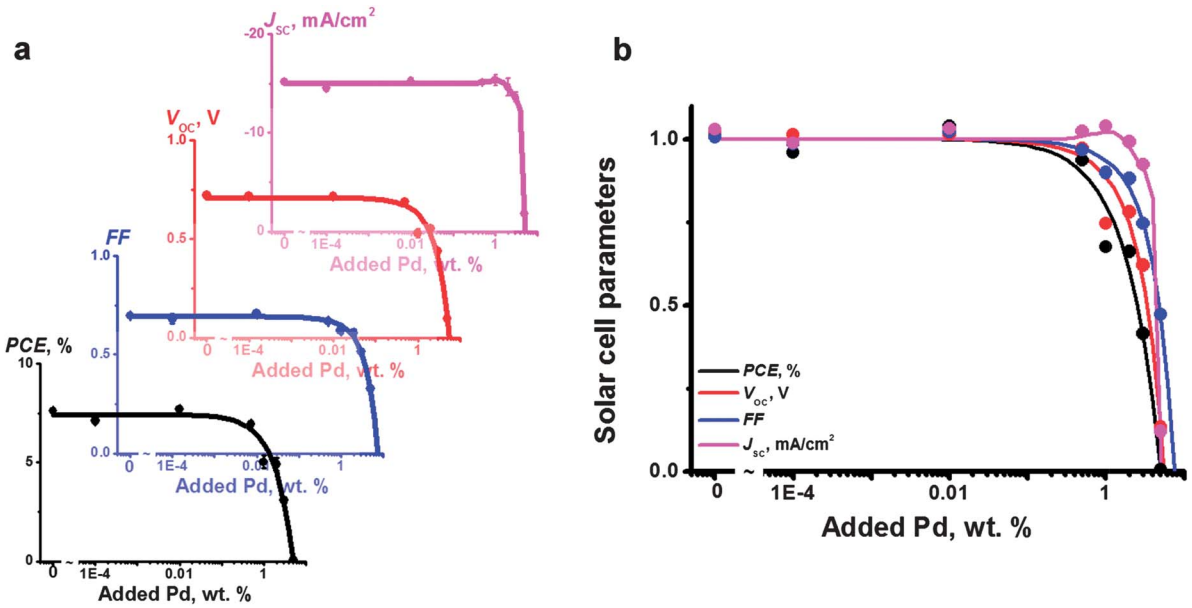

Fig. 3 (a) PTB7/$PC_{71}BM$ solar cell device parameters (J_{sc}, V_{oc}, FF, PCE) as a function of added palladium catalyst concentration in solution. (b) Normalized solar cell device parameters *vs.* added palladium catalyst concentration, showing the relative effects on each parameter. All lines are guides to the eye. Spin speed was 1000 rpm for all devices. Error bars represent the spread of values from an average of 3–4 devices.

concentrations. Interestingly, while J_{sc} does also eventually suffer from the presence of palladium, it first shows a slight improvement around 1% added catalyst concentration, a phenomenon that has been reported previously with P3HT/PCBM,[22] and is likely evidence of increased conductivity in the film, which is eventually overcome by phenomena damaging to device performance. The addition of less than 1 wt% of palladium catalyst to the solution does not significantly affect the performance of PTB7-based devices. The likely explanation for this apparent tolerance for impurity is the (previously unknown) presence of Pd-based derivatives in the material as purchased. Deterioration of performance is unlikely to be detected until the concentration of added Pd-based derivatives in the OPV material is larger than the original concentration of palladium catalyst poisoning the solid film. It is important to note that the concentration of $Pd(PPh_3)_4$ catalyst in the films cast from these solutions may not match that in the condensed phase due to differences in solubility between the polymer and the catalyst compound. The greater solubility of the catalyst means that, during casting, a relatively larger fraction of the catalyst will be

ejected from the film with excess solvent compared with the polymer, effectively decreasing the palladium concentration in the final film. The amount of palladium impurity in the active layer of the devices was quantified using the synchrotron-based X-ray fluorescence (XRF) technique.

XRF is a standard method for chemical analysis using ionization of inner atomic shells and energy dispersive spectroscopy of emitted characteristic X-rays. Because of the significant background in electron-induced X-ray emission and the very low concentrations of metal atoms in the materials of interest, standard electron beam-based XRF techniques do not provide sufficient sensitivity to detect trace catalysts in OPV materials. X-ray induced XRF has a sensitivity several orders of magnitude better than electron-based methods due to the absence of bremsstrahlung background generated by the exciting electron beam.[26] Thus, we used synchrotron-based XRF to measure the amount of residual palladium in PTB7/$PC_{71}BM$ films. We adopt the strategy of introducing known quantities of pristine tetrakis(triphenylphosphine)palladium(0) catalyst and measuring the emitted XRF signal (Fig. 4b and c). Fig. 4d depicts this relationship quantitatively. Under the assumption that the density of the polymer/fullerene blend is 2 g cm^{-3}, solid content of the solution with 1, 2, 3, and 5 wt% of added palladium catalyst should have 1.84, 3.66, 5.50, and 9.18 mg of palladium metal per cubic centimeter, respectively (Table 1). Since the fluorescence signal is directly proportional to the amount of palladium in the sample, palladium depletion of the PTB7/$PC_{71}BM$ film after spin-coating is evident. This observation contradicts the common assumption made by OPV researchers that the solution composition is equivalent to the composition of the final spin-coated film. XRF data can be used to determine the palladium concentration of the original PTB7 material by extrapolating back to the ordinate axis, which we calculate to be 0.16 ± 0.08 mg cm^{-3}.

Table 1 Palladium concentration in PTB7-based solutions and thin films

$Pd(PPh_3)_4$ (wt%)	Pd in solution (wt%)	Solid Pd content in solution (mg cm^{-3})	Pd in film (mg cm^{-3}) from XRF	Average Pd–Pd distance (nm)
0.0	—	—	0.16 ± 0.08	10.3
1.0	0.092	1.84	0.45 ± 0.05	7.3
2.0	0.183	3.66	0.64 ± 0.06	6.5
3.0	0.275	5.50	1.07 ± 0.08	5.5
5.0	0.459	9.18	1.51 ± 0.07	4.9

Fig. 3 shows that deterioration of device properties is noticeable at less than 1 wt% of added palladium catalyst (~0.5 mg cm^{-3}). The fact that added palladium begins to display a noticeable effect at approximately the concentration of palladium we measure as being present in the original "pure" material suggests that the original palladium is influencing the device and that improvement might be possible through efforts to further purify this polymer prior to device fabrication.

It is apparent that the effect of palladium impurities in OPV devices is primarily that of introducing trap sites, which become filled with photogenerated charges. The electronic effect of traps in polymer electronics,[27] and organic solar cells specifically,[28–30] is well documented. Electrons become trapped more easily than holes in organic systems because of their low charge density,[28] and then holes transporting in the vicinity of these sites can recombine with the trapped electrons. (A trapped electron may also detrap *via* a phonon- or photon-assisted transition, thereby returning to the LUMO.) Trap-assisted

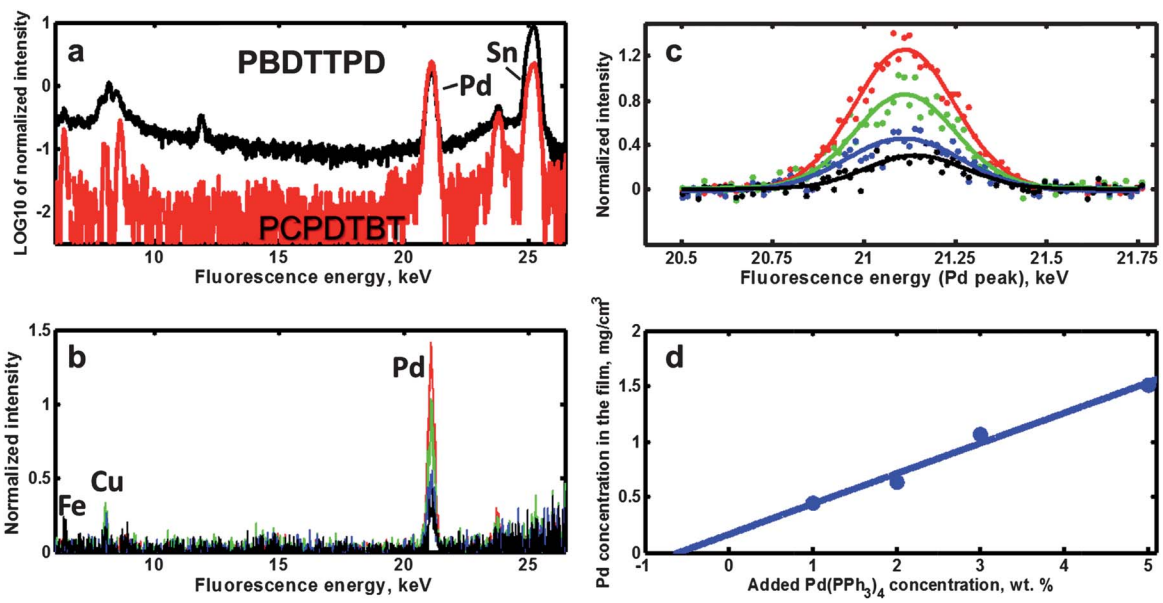

Fig. 4 (a) Thickness-normalized synchrotron X-ray fluorescence spectra of PBDTTPD and PCPDTBT conjugated polymer films. (b) Thickness-normalized XRF survey spectra of PTB7/$PC_{71}BM$ films with varying amounts of added catalyst. (c) Palladium Kα peak from PTB7/$PC_{71}BM$ samples with various amounts of added catalyst (color scheme: red – 5 wt%; green – 3 wt%; blue – 2 wt%; black – 1 wt%). Gaussian fits are a guide to the eye. (d) Plot of palladium concentration in the film as quantified using XRF *vs.* amount of added catalyst. Standard deviations (two sigma, 95% confidence interval) of Pd concentration in the film derived from the photon statistics are smaller than the size of the markers in (d).

 This journal is © The Royal Society of Chemistry 2013

recombination can, in some cases, be a dominant contributor to device performance issues, even outweighing intrinsic bimolecular recombination when the trap density is sufficiently high. While more sophisticated models have been proposed, often the Shockley-Read-Hall (SRH) description will suffice to describe this effect:[31]

$$R_t = \frac{n_e n_h - n_i^2}{\tau_e(n_e + n_{e,trap}) + \tau_h(n_h + n_{h,trap})} \quad (1)$$

where R_t is the SRH recombination rate, n_e is the density of electrons in the LUMO of the fullerene, n_h is the density of holes in the HOMO of the polymer, n_i is the intrinsic carrier density at equilibrium, $n_{e(h),trap}$ is the density of trapped electrons (holes), and $\tau_{e(h)}$ is the recombination lifetime of mobile electrons (holes). Reduction in steady-state current is directly connected to this phenomenon, but there are also indirect effects including build-up of space charge (which also limits current by suppressing transport with a field) and reduction in open circuit voltage. Following arguments outlined in the literature[2] and based on SRH theory, V_{oc} is expected to be reduced as trap-assisted recombination lowers the average occupation density of the LUMO, that is, the Fermi level is lowered.

In order to track the dynamics of the trap-assisted recombination process, transient absorption spectroscopy was performed on PTB7/$PC_{71}BM$ films identical to those used in the device measurements. A reflection geometry was adopted in order to probe films with a top electrode in place. Exciting the donor (polymer) and probing in the near infrared region, one can track a broad induced absorption peaking around 1000 nm that is correlated with the presence of charge carriers in the film (Fig. 5a). As the spectral feature is so broad, we integrate over a wide wavelength range when tracking the dynamics. Fig. 5b displays these dynamics for the pristine PTB7/$PC_{71}BM$ film (0% added $Pd(PPh_3)_4$ catalyst) and the film with 5% added catalyst, corresponding to the device exhibiting substantial degradation in performance attributed to trap-assisted recombination. For pump–probe delays in excess of 10 ns, the data are fit to a single exponential resulting in time constants of $t_1 = 86$ ns $\pm$ 6 and 57 ns $\pm$ 3 for the pristine and 5% samples, respectively. Clearly, the film containing a greater concentration of Pd material shows substantially faster decay of the NIR induced absorption, which we attribute to the loss of charge carriers to recombination.

If one assumes that the palladium species remaining in the active layer are isotropically distributed, it is possible to estimate the average spacing between palladium atoms based on the concentration. It is important to note that polymer-rich and fullerene-rich phases[32] will likely have different concentrations of palladium due to differing affinities and that palladium catalysts are known to undergo chemical transformations during synthetic processes, including the formation of metal nanoparticles, but some intriguing concurrences can be observed in this system where the majority of the palladium is likely still in its pristine state since it has been artificially added after synthesis is complete. Table 1 provides an estimate of the inter-palladium distance for different amounts of added palladium catalyst compound, which ranges from ~10 nm in the pristine material to ~5 nm in the system with 5 wt% catalyst in

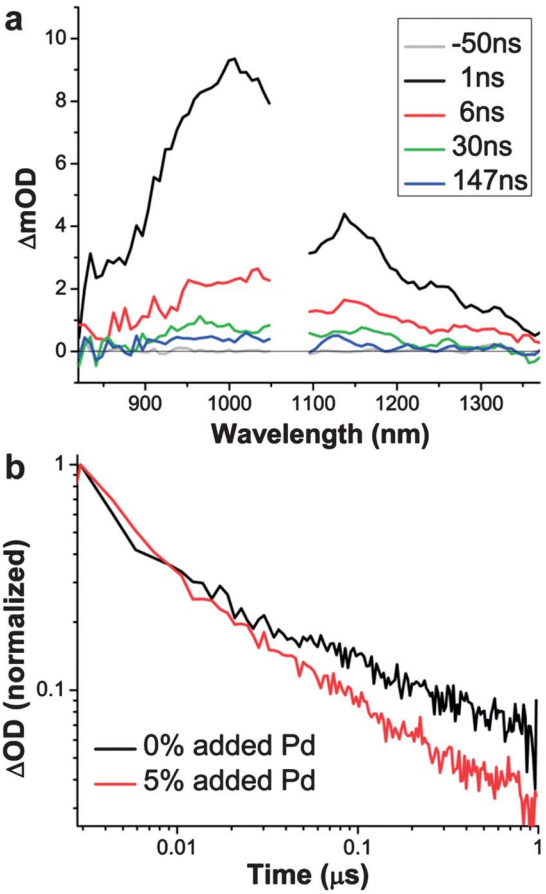

Fig. 5 (a) Transient absorption spectra at various pump–probe delay times (650 nm excitation) of PTB7/$PC_{71}BM$ film with 5% added $Pd(PPh_3)_4$ catalyst; spectra of films with different amounts of catalyst were qualitatively similar. The blanked region in the center is due to scatter from the 1064 nm laser used to generate the white light probe. (b) Transient absorption dynamics spectrally integrated from 1046–820 nm for samples with no added $Pd(PPh_3)_4$ catalyst and with 5% added catalyst.

solution. The concentration range at which optoelectronic function of the material in OPV device is first affected (~0.4 mg cm^{-3}) corresponds to an average palladium spacing of ~8 nm. This value is comparable to the exciton diffusion distance in polymeric materials[33] and several times the typical intersite charge hopping distance in disordered organic semiconductors (~1 nm).[34] Though conceivably coincidental, it is possible that the correspondence between the exciton diffusion distance and the trace impurity spacing reflects a trapping mechanism at play. Perhaps when it is likely that a substantial majority of excitons will encounter a metal atom trap site prior to charge separation, the traps play a dominant role in the separation process itself. Ongoing studies are directed toward elucidating the spatial distribution of the metallic impurities and, thereby, deciphering their mechanistic role in device function.

Other high-performance OPV donors, each of which achieves 6–9% power conversion efficiency in optimized OPV devices, depicted in Fig. 1 are also synthesized *via* Stille coupling involving palladium compounds. Note that unreacted monomer and chain ends will retain tin and bromine in the end product, which we also detected using the synchrotron XRF

technique. XRF spectra of these polymers, as received from the supplier, are shown in Fig. 4. These data are normalized to the film thickness (measured using X-ray reflectivity; see ESI†) in order to provide a quantitative relative measure of the residual metal impurities between these different materials. From the area under the palladium fluorescence peak, we find that the pristine PBDTTPD and PCPDTBT films contain 2.1 ± 0.02 and 2.7 ± 0.03 mg cm^{-3} palladium concentration, which is significantly higher than that observed in PTB7 films (~0.16 ± 0.08 mg cm^{-3}). Thus, palladium contamination seems to be a pervasive issue with high-performance polymers synthesized using Stille coupling reactions.

Experimental details

Materials

PTB7 (poly[[4,8-bis[(2-ethylhexyl)oxy]benzo[1,2-*b*:4,5-*b*′]dithiophene-2,6-diyl][3-fluoro-2-[(2-ethylhexyl)carbonyl]thieno[3,4-*b*]thiophene-diyl]]), PBDTTPD ([poly([4,8-di(2-ethylhexyloxyl)benzo[1,2-*b*:4,5-*b*′]dithiophene]-2,6-diyl)-*alt*-([5-octylthieno[3,4-*c*]pyrrole-4,6-dione]-1,3-diyl)]]), and PCPDTBT (poly[2,6-(4,4-bis-(2-ethylhexyl)-4*H*-cyclopenta [2,1-*b*;3,4-*b*′]dithiophene)-*alt*-4,7(2,1,3-benzothiadiazole)]) polymers were purchased from 1-Material (Québec, Canada). [6,6]-Phenyl-C_{71}-butyric acid methyl ester ($PC_{71}BM$, >99%) was obtained from American Dye Source. 1,8-Diiodooctane (DIO) (98%, contains copper as stabilizer), tetrakis-(triphenylphosphine)palladium(0) ($Pd(PPh_3)_4$, 99%), and 1,2-dichlorobenzene (DCB, 99% purity anhydrous) were purchased from Aldrich. Poly(3,4-ethylenedioxythiophene) poly(styrenesulfonate) (PEDOT:PSS) was obtained from Heraeus (Clevious P VP AI 4083). Indium tin oxide (ITO)-coated glass substrates were supplied by Delta Technologies, Ltd. (25 Ω sq^{-1}). All materials were used as received unless otherwise noted.

X-ray fluorescence

Trace elements in the thin films were measured using the hard X-ray fluorescence microprobe at beamline 2-ID-D of the Advanced Photon Source (APS) at Argonne National Laboratory. Intense hard X-rays were produced by an undulator source. X-rays with a photon energy of 30 keV X-rays were selected using a Si ⟨111⟩ crystal monochromator and delivered to the sample with a beam spot size of 0.2 mm (*h*) × 0.2 mm (*v*), without use of microfocusing X-ray optics. Fluorescence signals emitted from the samples were collected using an energy dispersive detector positioned at 90 degrees with respect to the incident beam. The elemental concentration was determined by comparing the signal intensity emitted by the samples with that emitted from a standard with known Pd area concentration (Thin film XRF reference RF7-200-S2371, AXO Dresden GmbH), under identical experimental condition.[35] The background level was determined by performing the same measurement on a blank sample substrate (Si_3N_4 membrane film).

X-ray reflectivity

X-ray reflectivity (XRR) measurements were performed using an avalanche photodiode detector at beamline 8-ID-E at the APS, Argonne.[36] The photon energy of the incident X-rays was 7.35 keV, with a wavelength of $\lambda = 1.6868$ Å and a beam size of ~100 μm (*h*) × 50 μm (*v*). Positive longitudinal diffuse background scattering was measured with the incident angle offset from the specular condition by +0.1° and subtracted from the specular reflectivity at each incident angle. The samples for XRR measurements consisted of the photoactive layer, without the electron transport, top contact and encapsulating layers, but were prepared on PEDOT:PSS modified Si substrates under otherwise the same conditions as those used for fabrication of OPV devices. Film thickness calculations were performed using the MOTOFIT analysis package[37] running on IGOR Pro.

Device fabrication

Detailed description of the device fabrication procedure can be found elsewhere.[5] The PEDOT:PSS hole-transport layer was prepared by spin coating at 1000 rpm in ambient conditions on clean 1 in. × 1 in. ITO-coated glass substrates followed by annealing in a nitrogen-filled glove box at 150 °C for 15 min. This procedure typically results in a 50 nm thick PEDOT:PSS layer. The active layer was spin coated from PTB7-based solution at different spin rates (500 rpm, 1000 rpm, 1500 rpm, 2000 rpm, 3000 rpm). The solutions used for active layer preparation contained PTB7, $PC_{71}BM$, DIO, $Pd(PPh_3)_4$, and DCB. To prepare 1 mL of solution, 10 mg of PTB7 and 15 mg of $PC_{71}BM$ were dissolved in DCB–DIO mixture (3% DIO by volume). Addition of 0.000001 mg, 0.00001 mg, 0.001 mg, 0.05 mg, 0.1 mg, 0.2 mg, 0.3 mg, 0.5 mg of $Pd(PPh_3)_4$ created solutions with 10^{-5}, 10^{-4}, 10^{-2}, 0.5, 1, 2, 3, 5 weight% of $Pd(PPh_3)_4$. After deposition of hole-transport and active layers, an electron-transport layer was deposited using thermal evaporation of Ca (50 nm) and Al (50 nm) layers under vacuum (3×10^{-6} mbar or better). Resulting devices consisted of ITO/PEDOT:PSS/PTB7:$PC_{71}BM$:$Pd(PPh_3)_4$/Ca/Al. Encapsulation of devices was performed inside the glove box. 170–250 μm of glass (cover glass slides from Fischer Scientific, 12-540-C) was used as a cover material and silicone (McMaster-Carr, #7615A51; 2.5 mil (~70 μm) thickness) as an adhesive material. Silicon adhesive was applied to a glass sheet, which was subsequently applied to an ITO/glass substrate with photovoltaic devices ensuring complete coverage of the solar cells. Small pressure was applied by fingers to the encapsulation layer to remove N_2 bubbles and ensure good sealing of the devices.

Device characterization

The active device area was limited to 4.87 mm^2 by a shadow mask. Current–voltage (*I*–*V*) curves were recorded using a Keithley 2420 source-measure unit. The photocurrent was measured under AM 1.5 G illumination at 100 mW cm^{-2} under a Newport Oriel Solar Simulator with a 300 Watt Xenon source and 2 in. × 2 in. illuminated area. Prior to each measurement, the light intensity was adjusted to ensure constant repeatable light power density using NREL-calibrated photodiodes. Standard solar cell parameters, such as power conversion efficiency, fill factor, and short-circuit current, were calculated from *J*–*V* curves of the solar cell under illumination using conventional procedures.

 This journal is © The Royal Society of Chemistry 2013

Transient absorption spectroscopy

Transient absorption measurements were performed using an Ultrafast Systems EOS spectrometer. In these measurements, a Spectra-Physics amplified titanium:sapphire laser operating at 1 kHz and 120 fs pumped a TOPAS-C optical parametric amplifier to produce a 650 nm pump beam. The pump beam was adjusted to 400 nJ per pulse and focused onto the sample with a 750 μm beam diameter. The probe pulse was generated *via* self-phase modulation of an independent Nd:YAG laser in a photonic crystal fiber. The temporal delay between the pump and probe was determined with a digital analyzer. Samples were continuously translated during optical measurements.

Conclusions

Variation in trace impurities from one synthetic batch to the next of conjugated polymers is a ubiquitous yet often overlooked challenge in obtaining consistently high efficiency in organic photovoltaics. We have shown that, using synchrotron X-ray fluorescence, it is possible not only to identify which impurities are present, but also to quantitatively measure their concentration at levels well below those detectable using traditional techniques. Our focus in this study was on residual palladium catalyst used in Stille coupling reactions, which we link directly to trap-assisted recombination in PTB7/$PC_{71}BM$ solar cells, but it is likely that other metal impurities also play a role in optoelectronic function and will be the subject of ongoing studies. With synchrotron XRF, researchers can analytically characterize batch variations in conjugated polymer syntheses and select those materials that will have minimal impact on recombination and, therefore, performance. Fortunately, purification methodologies have been reported for removal of transition metal impurities from conjugated organic systems.[15,38] Coupled with the ability to detect trace quantities, these strategies will enable reproducible, high-performance processing.

Acknowledgements

This work was performed, in part, at the Center for Nanoscale Materials, a U.S. Department of Energy, Office of Science, Office of Basic Energy Sciences User Facility under Contract no. DE-AC02-06CH11357. Use of the Advanced Photon Source (APS) at Argonne National Laboratory was supported by the U.S. Department of Energy, Office of Science, Office of Basic Energy Sciences, under Contract no. DE-AC02-06CH11357. MPN is grateful to the Director's Fellowship Program for financial support.

Notes and references

1 W. L. Leong, G. C. Welch, L. G. Kaake, C. J. Takacs, Y. Sun, G. C. Bazan and A. J. Heeger, *Chem. Sci.*, 2012, **3**, 2103–2109.
2 S. R. Cowan, W. L. Leong, N. Banerji, G. Dennler and A. J. Heeger, *Adv. Funct. Mater.*, 2011, **21**, 3083–3092.
3 F. C. Krebs, R. B. Nyberg and M. Jørgensen, *Chem. Mater.*, 2004, **16**, 1313–1318.
4 F. He, W. Wang, W. Chen, T. Xu, S. B. Darling, J. Strzalka, Y. Liu and L. Yu, *J. Am. Chem. Soc.*, 2011, **133**, 3284–3287.
5 Y. Liang, Z. Xu, J. Xia, S.-T. Tsai, Y. Wu, G. Li, C. Ray and L. Yu, *Adv. Mater.*, 2010, **22**, E135–E138.
6 Y.-H. Chen, L.-Y. Lin, C.-W. Lu, F. Lin, Z.-Y. Huang, H.-W. Lin, P.-H. Wang, Y.-H. Liu, K.-T. Wong, J. Wen, D. J. Miller and S. B. Darling, *J. Am. Chem. Soc.*, 2012, **134**, 13616–13623.
7 L. Dou, J. You, J. Yang, C.-C. Chen, Y. He, S. Murase, T. Moriarty, K. Emery, G. Li and Y. Yang, *Nat. Photonics*, 2011, **6**, 180–185.
8 H. X. Zhou, L. Q. Yang and W. You, *Macromolecules*, 2012, **45**, 607–632.
9 Y. M. Sun, G. C. Welch, W. L. Leong, C. J. Takacs, G. C. Bazan and A. J. Heeger, *Nat. Mater.*, 2012, **11**, 44–48.
10 R. Sondergaard, M. Hosel, D. Angmo, T. T. Larsen-Olsen and F. C. Krebs, *Mater Today*, 2012, **15**, 36–49.
11 D. Yue, P. Khatav, F. You and S. B. Darling, *Energy Environ. Sci.*, 2012, **5**, 9163–9172.
12 B. Carsten, F. He, H. J. Son, T. Xu and L. Yu, *Chem. Rev.*, 2011, **111**, 1493–1528.
13 D. Milstein and J. K. Stille, *J. Am. Chem. Soc.*, 1978, **100**, 3636–3638.
14 A. Suzuki, *Acc. Chem. Res.*, 1982, **15**, 178–184.
15 K. T. Nielsen, K. Bechgaard and F. C. Krebs, *Macromolecules*, 2005, **38**, 658–659.
16 K. Sonogashira, Y. Tohda and N. Hagihara, *Tetrahedron Lett.*, 1975, **16**, 4467–4470.
17 *Design and Synthesis of Conjugated Polymers*, ed. M. Leclerc and J. F. Morin, Wiley, 2010.
18 K. T. Nielsen, H. Spanggaard and F. C. Krebs, *Macromolecules*, 2005, **38**, 1180–1189.
19 P. A. Troshin, D. K. Susarova, Y. L. Moskvin, I. E. Kuznetsov, S. A. Ponomarenko, E. N. Myshkovskaya, K. A. Zacharcheva, A. A. Balakai, S. D. Babenko and V. F. Razumov, *Adv. Funct. Mater.*, 2010, **20**, 4351–4357.
20 M. Urien, G. Wantz, E. Cloutet, L. Hirsch, P. Tardy, L. Vignau, H. Cramail and J.-P. Parneix, *Org. Electron.*, 2007, **8**, 727–734.
21 S. S. Pandey, W. Takashima, S. Nagamatsu and K. Kaneto, *IEICE Trans. Electron.*, 2000, **E83-C**, 1088–1093.
22 A. Saeki, M. Tsuji and S. Seki, *Adv. Energy Mater.*, 2011, **1**, 661–669.
23 Y. Liang and L. Yu, *Acc. Chem. Res.*, 2010, **43**, 1227–1236.
24 Y. Zou, A. Najari, P. Berrouard, S. Beaupré, B. R. Aïch, Y. Tao and M. Leclerc, *J. Am. Chem. Soc.*, 2010, **132**, 5330–5331.
25 C. Soci, I.-W. Hwang, D. Moses, Z. Zhu, D. Waller, R. Gaudiana, C. J. Brabec and A. J. Heeger, *Adv. Funct. Mater.*, 2007, **17**, 632–636.
26 C. J. Sparks, in *Synchrotron Radiation Research*, ed. H. Winick and S. Doniach, Plenum, 1980, pp. 459–512.
27 D. M. Taylor, *IEEE Trans. Dielectr. Electr. Insul.*, 2006, **13**, 1063–1073.
28 M. M. Mandoc, W. Veurman, L. J. A. Koster, M. M. Koetse, J. Sweelssen, B. de Boer and P. W. M. Blom, *J. Appl. Phys.*, 2007, **101**, 104512.

This journal is © The Royal Society of Chemistry 2013

29 M. M. Mandoc, F. B. Kooistra, J. C. Hummelen, B. de Boer and P. W. M. Blom, *Appl. Phys. Lett.*, 2007, **91**, 263505.
30 C. R. McNeill and N. C. Greenham, *Appl. Phys. Lett.*, 2008, **93**, 203310.
31 S. R. Cowan, A. Roy and A. J. Heeger, *Phys. Rev. B: Condens. Matter Mater. Phys.*, 2010, **82**, 245207.
32 W. Chen, T. Xu, F. He, W. Wang, C. Wang, J. Strzalka, Y. Liu, J. Wen, D. J. Miller, J. Chen, K. Hong, L. Yu and S. B. Darling, *Nano Lett.*, 2011, **11**, 3707–3713.
33 M. Knupfer, *Appl. Phys. A*, 2003, **77**, 623–626.
34 A. Saeki, Y. Koizumi, T. Aida and S. Seki, *Acc. Chem. Res.*, 2012, **45**, 1193–1202.
35 R. Jenkins, R. W. Gould and D. Gedcke, *Quantitative X-ray Spectrometry: 20 (Practical Spectroscopy)*, Marcel Dekker, Inc., New York, 1995.
36 Z. Jiang, X. Li, J. Strzalka, M. Sprung, T. Sun, A. R. Sandy, S. Narayanan, D. R. Lee and J. Wang, *J. Synchrotron Radiat.*, 2012, **19**, 627–636.
37 A. J. Nelson, *J. Appl. Crystallogr.*, 2006, **39**, 273–276.
38 K. T. Nielsen, K. Bechgaard and F. C. Krebs, *Synthesis*, 2006, **2006**, 1639–1644.

 This journal is © The Royal Society of Chemistry 2013